THE ASTRONOMICAL JOURNAL, 120:752–762, 2000 August

ON THE SIZE AND LUMINOSITY VERSUS VELOCITY DISPERSION CORRELATIONS FROM THE GIANT H II REGIONS IN THE IRREGULAR GALAXY NGC 4449

ORIOL FUENTES-MASIP AND CASIANA MUÑOZ-TUÑÓN
Instituto de Astrofísica de Canarias, Via Lactea, E-38200 La Laguna, Tenerife, Spain; ofm@iac.es, cmt@iac.es
HÉCTOR O. CASTAÑEDA
Observatorio Astronómico Nacional, Universidad Nacional Autónomico de México, Apdo. Postal 877, 22860 Ensenada, BC, 22800 Mexico; hcastane@bufadora.astrosen.unam.mx
AND
GUILLERMO TENORIO-TAGLE
Instituto Nacional de Astrofísica, Optica y Electrónica, Apdo. Postal 51216, 72000 Puebla, Pue. Mexico; gtt@inaoep.mx
Received 2000 March 9; accepted 2000 May 5

ABSTRACT

Here we present the size and luminosity versus velocity dispersion empirical correlations for the giant H II regions in the large irregular galaxy NGC 4449. We show that correlations only hold for nebulae with a surface brightness higher than 2×10^{35} ergs s^{-1} pc^{-2} in Hα and with a supersonic single-line Gaussian profile. The exponents of the fits are consistent with virial mechanisms. A comparison with the results from other studies that have only used first-ranked giant H II regions from a variety of star-forming galaxies is also given.

Key words: galaxies: individual (NGC 4449) — H II regions — turbulence

1. INTRODUCTION

Giant H II regions are found in high luminosity spirals and in irregular galaxies. Typically they present a diameter larger than 100 pc and an Hα luminosity of the order of 10^{39} ergs s^{-1}, which implies some 10^{51} *uv* photons s^{-1} and thus a couple of hundreds of massive OB stars (Kennicutt 1984). The total amount of ionized gas is of the order of 10^5–10^6 $M_\odot$ and the average mean density is about 1–10 particles cm^{-3}.

Since the work of Smith & Weedman (1970), it became clear that an important intrinsic characteristic of these regions was the fact that they present supersonic velocity dispersions ($\sigma \geq c_{\rm H\,II} = (kT_{\rm H\,II}\,\mu m^{-1})^{0.5} = 12.85$ km s^{-1} for $T_{\rm H\,II} = 10^4$ K; where k is the Boltzmann constant, m is the hydrogen mass, and μ the mean molecular weight of up to some 40 km s^{-1}. This has become a central issue in interstellar medium studies. First because it has been shown that σ correlates with both the size and the luminosity of the regions, facts that have allowed for their use as a distance indicator. Also, because it has led to profound searches of possible ways to sustain the supersonic motions, which unavoidably should lead to the formation of strong radiative shocks and thus are expected to decay rapidly.

There have been several attempts to use giant H II regions as extragalactic distance indicators making use of their large size and luminosity and the properties of their host galaxies (Gum & de Vaucouleurs 1953; Sérsic 1960; Sandage & Tamman 1974; Kennicutt 1979, 1984, 1988). Melnick (1977) and Terlevich & Melnick (1981) found however, that both the size and luminosity of giant H II regions correlate with another intrinsic property of the nebulae: their velocity dispersion. The correlation between size and σ ($R \propto \sigma^2$), and luminosity and σ ($L\sigma^4$), were also noted by Terlevich & Melnick (1981) to be similar to the relations that hold in virialized self-gravitating stellar systems, such as globular clusters, spiral bulges, and the nuclei of elliptical galaxies. This fact allowed them to postulate that the observed σ-values reflect the total mass of the systems. The correlations have now been explored by several groups and although the study of Gallagher & Hunter (1983) did not confirm them in a sample which included H II regions with subsonic line-widths, most other studies, taking into consideration H II regions with supersonic σ-values, have reported correlations (Hippelein 1986; Roy, Arsenault, & Joncas 1986; Melnick et al. 1987, 1988; Rozas et al. 1998), although with slopes slightly different to the ones originally found by Terlevich & Melnick (1981).

Several ways of broadening the emission-line profiles have been proposed to explain the supersonic line widths detected in giant H II regions. The proposed mechanisms split into two main groups: gravitational models and those where the line broadening is due to the mechanical energy injected by massive stars. In the gravitational models (see Terlevich & Melnick 1981), the detected Gaussian line profiles are believed to be related to virialized motions within the H II regions, and thus $\sigma \sim (GM/R^2)^{0.5}$ as in the most recent *cometary stirring model* (CSM) of Tenorio-Tagle et al. (1993). In the CSM it is a collection of low-mass stars, which, as they move in the gravitational potential of a recently formed starburst and develop their stellar winds, become able to enhance their cross-section and persistently shock and stir the gas left from the star-forming process.

A completely different broadening mechanism involves the combined action of several unresolved stellar wind-driven expanding shells and filaments (see Dyson 1979 and Tenorio-Tagle et al. 1996). Note that all models confront serious difficulties and also that despite the evidence of multiple shells in giant H II regions (see Chu & Kennicutt 1994) the wind-driven broadening models have made no attempt at explaining the observed correlations. For a summary of all possible interpretations see Melnick, Tenario-Tagle, & Terlevich (1999) and Muñoz-Tuñón et al. (1996).

Here we analyze the results obtained for the giant H II regions of the irregular galaxy NGC 4449 (see Fuentes-Masip, Castañeda, & Muñoz-Tuñón 2000, hereafter Paper

I). This has been selected as an ideal target because it is a nearby galaxy at a distance of 5 Mpc (Sandage & Tammann 1975; Aaronson & Mould 1983). Also because of its giant size (diameter $\sim$ 5 kpc) and especially for the large number of giant H II regions that it presents. 252 H II regions have been cataloged by Sabbadin & Bianchini (1979) and a large proportion of them present supersonic σ-values, particularly those occupying the most central zone (Hartmann, Geller, & Huchra 1986). This is the first time that an irregular galaxy has been selected for this kind of study. Note that also the work of Arsenault, Roy, & Boulesteix (1990) on the spiral galaxy NGC 4321 has addressed the existence of the empirical correlations for giant H II regions in a single galaxy. This is an important issue if one is to eliminate major sources of error in the determination of luminosities and sizes arising from uncertainties in the distance to different targets. For the H II regions in the giant irregular NGC 4449 we can also be sure that our sample of H II regions is very homogeneous, as these evolve in the absence of a spiral structure and in galactic zones with very similar global kinematics. The lack of such possible contamination is believed to lead to a simpler study. Section 2 presents a summary of the observations and data reduction, as well as an estimate of possible sources of error in the determination of all different parameters. Section 2 also contains our catalog of H II regions in NGC 4449. Section 3 is devoted to the data analysis and the empirical correlations and §§ 4 and 5 compare our work with former studies and give a summary and our final remarks.

2. THE H II REGIONS SAMPLE

TAURUS-II Fabry-Perot imaging spectroscopy was carried out on NGC 4449. The observations were taken at the 4.2 m, William Herschel Telescope (WHT) at the Observatorio del Roque de los Muchachos (ORM) at La Palma in the Canary Islands. With this setup simultaneous spectra of NGC 4449 with good spectral and spatial resolution were obtained; four data cubes, two in Hα and two in [O III], covering the central, $80'' \times 80''$ region of NGC 4449. The two fields in each wavelength overlapped and thus allow for a comparison of common sectors. The observed area contains the largest and most luminous H II regions of the galaxy, with an extremely high fraction of them presenting supersonic emission-line widths.

The output from this observational setup, after phase correction and calibration,[1] is a set of three-dimensional data cubes where x and y are the spatial plane and z the wavelength (etalon step) sampling. The data cube dimensions were (245, 217, 100) and the chosen etalon free spectral range (FSR) was 13.4 Å, or 610 km s^{-1} in Hα ($\lambda = 6562.8$ Å) and 7.78 Å, or 466 km s^{-1} in [O III] ($\lambda = 5006.8$ Å). The spatial scale was $0''.26$ pixel^{-1}, or 6.30 pc at the distance on NGC 4449. The exposure time for each data cube was 1 hr. Spectral scanning in Hα was $\Delta\lambda$/step = 0.20 Å, equivalent to 9.11 km s^{-1}, and $\Delta\lambda$/step = 0.13 Å, equivalent to 7.7 km s^{-1} in [O III].

Interference filters with a FWHM = 15 Å were used to isolate one interference order of the Fabry-Perot. The image photon counting system (IPCS) was employed as detector. With the IPCS the 100 planes are scanned continuously with 10 ms exposures to average effects of atmospheric transmission variations during the 1 hr exposure time. In this way, changes of seeing occurring during the exposure time do not preferentially affect a particular plane, what would modify the emission-line profile. During the observations the seeing was always below $1''.0$. Flux calibration was made using Hα and [O III] CCD images taken at the Jacobus Kapteyn 1 m telescope, also at the ORM. A complete description of the observations and data reduction is given in Fuentes-Masip (1997) and in Paper I.

A phase-corrected and wavelength-calibrated TAURUS data cube contains a total of 53,165 spectra, from an area of 1 arcmin^2. The data analysis was carried out using specific software, MATADOR (see details in Gavryusev & Muñoz-Tuñón 1996 and Muñoz-Tuñón et al. 1995).

The emission in the 100 wavelength planes was added up to produce the so-called *collapsed* maps. The underlying continuum was fitted in the data cubes and then subtracted to the collapsed maps in order to obtain the continuum-free emission maps.

The high density of nebulae per unit area, together with the important diffuse luminosity engulfing the H II regions (Malumuth, Williams, & Schommer 1986; Muñoz-Tuñón et al. 1995, and references therein) made it particularly difficult to catalog and determine the integrated parameters of all H II regions. In fact, a detailed analysis was necessary to sort out each individual region, see Paper I. All different procedures used in the literature were also tried and tested: visual analysis (e.g., Sandage & Tammann 1974; Hodge 1976, 1983; Sabbandin & Bianchini 1979), isophotal threshold (Kennicutt 1979), emission-line width gradients (Gallagher & Hunter 1983; Muñoz-Tuñón 1994). Also FOCAS (faint objects classification and analysis system, developed by Valdez, within the IRAF[2] environment), which allows for the detection of relative maxima in an image, was used. As a diagnosis of the reliability of the findings the cumulative distribution function of sizes was also worked out. However, none of these techniques, which may be excellent for the study of H II regions in spiral galaxies, provided satisfactory results for identifying the H II regions of NGC 4449.

The procedure finally adopted consisted of the following. First, the diffuse luminosity was subtracted. Then, all relative maxima were detected by means of FOCAS. This was followed by a final extrapolation of the corresponding luminosity profiles to the background level. The H II region parameters have then been obtained as if the nebulae were isolated and located on a galaxy without any diffuse emission.

Regarding the errors determination, it was basically aimed at measuring the different reliability of the parameters derived for each H II region. The goal was to obtain relative weights for the nebulae in our sample concerning the parameters involved in the correlations between size or luminosity and velocity dispersion and in this way to be able to meaningfully correlate these parameters by taking these errors into account.

Because of this, we did not consider the error associated to the uncertainty in the distance to NGC 4449 or to the

[1] See TAURUS Data and How To Reduce It, available at http://www.ing.iac.es/~manuals/html_manuals/wht_instr/taurus/subsection1.4.0.1.3.html.

[2] IRAF is distributed by the National Optical Astronomy Observatories, which are operated by the Association of Universities for Research in Astronomy, Inc., under cooperative agreement with the National Science Foundation.

TABLE 1

H II Region Integrated Parameters for the Hα Data

ID (1)	v_{rad} (km s^{-1}) (2)	σ (km s^{-1}) (3)	$\epsilon(\sigma)$ (km s^{-1}) (4)	R (pc) (5)	$\epsilon(R)$ (pc) (6)	R_F (pc) (7)	$\epsilon(R_F)$ (pc) (8)	log SB (ergs s^{-1} pc^{-2}) (9)	log F (ergs s^{-1} cm^{-2}) (10)	log L (ergs s^{-1}) (11)	ϵ(log L) (ergs s^{-1}) (12)
63.....	224.6	14.0	2.5	19.9	14.1	10.6	10.5	35.1	−13.6	37.9	1.5
86.....	235.8	8.2	2.9	26.0	9.6	13.9	6.3	35.1	−13.3	38.2	1.6
* 89	217.2	14.6	2.3	66.3	9.4	38.2	6.0	34.9	−12.6	38.9	0.1
90.....	227.6	18.7	4.3	25.8	21.7	22.6	12.8	34.4	−13.6	37.9	1.3
99.....	211.9	17.2	2.5	53.4	30.8	35.0	25.0	34.7	−12.9	38.6	1.3
101	213.5	22.6	2.5	29.8	14.0	20.5	14.2	34.6	−13.4	38.1	1.7
*108	230.6	14.1	2.2	60.3	9.4	26.6	6.0	35.6	−12.3	39.2	0.1
113	237.7	16.1	2.9	21.4	12.2	11.2	8.7	35.1	−13.5	38.0	1.2
*114	235.3	12.6	2.3	57.4	9.4	31.5	6.0	35.0	−12.7	38.8	0.2
116	219.0	16.4	2.3	55.1	41.2	36.6	33.7	34.7	−12.8	38.6	1.1
*119	213.7	11.0	2.2	61.2	9.4	29.0	6.0	35.4	−12.4	39.1	0.1
125	225.2	3.9	3.3	53.0	12.2	27.6	7.8	35.1	−12.7	38.8	0.2
*128–129.....	229.1	16.8	2.4	65.0	9.7	41.2	6.5	34.8	−12.7	38.8	0.2
131	232.0	11.4	2.4	44.6	9.6	25.5	6.3	34.9	−12.9	38.4	0.4
*132	221.9	11.4	2.2	54.4	9.4	24.1	6.0	35.6	−12.4	39.1	0.1
*133	213.4	16.4	2.3	52.5	9.4	23.8	6.0	35.5	−12.5	39.0	0.1
134	225.8	3.7	3.5	37.8	29.8	23.0	22.7	34.8	−13.1	38.4	1.5
137	232.3	19.9	3.2	37.9	27.8	23.3	23.1	34.8	−13.1	38.3	1.6
138	219.7	17.2	2.6	13.2	11.5	6.2	5.4	35.4	−13.7	37.8	1.2
*146	220.3	17.4	2.3	77.3	9.9	44.0	6.5	34.9	−12.5	39.0	0.1
149	204.1	26.3	2.5	45.6	11.7	27.8	8.4	34.8	−13.0	38.3	0.5
150	221.4	27.9	2.5	63.6	18.4	36.1	12.3	34.9	−12.6	38.8	0.3
*151	222.2	27.7	2.4	88.8	9.8	46.9	6.3	35.1	−12.3	39.2	0.1
152	221.3	13.7	2.5	39.1	9.8	23.7	6.7	34.8	−13.1	38.4	1.8
*153–159.....	219.2	22.4	2.4	49.3	9.6	27.2	6.3	35.0	−12.8	38.6	0.3
161	240.5	29.5	3.0	30.6	9.6	20.3	6.8	34.7	−13.4	38.1	1.5
170	214.0	42.1	3.4	56.8	21.8	31.4	14.5	35.0	−12.7	38.7	0.3
178–190	228.3	19.2	2.6	38.6	26.2	22.6	20.2	34.9	−13.1	38.4	1.5
183	181.8	18.4	2.9	25.5	11.1	18.0	10.8	34.6	−13.5	37.9	1.9
191	201.9	27.7	2.7	41.6	15.5	27.2	13.2	34.7	−13.1	38.4	1.4
197	188.8	15.6	4.3	16.3	10.7	9.4	9.2	34.9	−13.8	37.7	1.4
198	211.6	32.8	2.6	60.7	11.9	40.9	9.1	34.7	−12.7	38.7	0.2
*203	188.6	20.6	2.5	56.6	9.5	31.5	6.1	35.0	−12.7	38.8	0.2
*208	197.6	23.0	2.4	52.8	9.4	25.5	6.0	35.3	−12.6	38.9	0.1
*212	212.3	22.0	2.3	74.6	9.4	45.1	6.1	34.9	−12.5	38.9	0.1
*220	183.4	19.3	2.4	74.3	9.7	32.4	6.1	35.6	−12.1	39.4	0.0
*222	208.3	26.6	2.3	101.8	10.6	50.9	6.6	35.2	−12.0	39.4	0.1
*226	198.0	20.7	2.3	73.4	10.0	34.8	6.3	35.4	−12.2	39.2	0.1
229	221.7	18.0	2.4	55.6	52.9	32.5	27.1	34.9	−12.8	38.7	2.0
234	194.1	24.1	2.5	43.2	25.2	26.9	20.4	34.8	−13.0	38.5	1.2
*h 61	227.1	19.3	2.2	85.9	12.4	41.8	7.4	35.3	−12.1	39.3	0.1
*h 66	195.2	21.5	2.2	108.1	13.2	50.7	7.6	35.4	−11.9	39.6	0.1
*Nucleus.....	230.3	25.9	2.3	112.9	9.4	49.0	6.0	35.6	−11.7	39.8	0.0
No ID.....	213.2	34.2	3.4	35.5	19.8	21.8	16.7	34.8	−13.2	38.3	1.0

Note.—Columns: (1) identification number, (2) radial velocity, (3)–(4) velocity dispersion and velocity dispersion error, (5)–(6) radius at a level 3 times higher than the standard deviation of the local background and error, (7)–(8) radius corresponding to the half width at half maximum of the luminosity profile and estimated error, (9) logarithm of the surface brightness, (10) logarithm of the flux (11)–(12) logarithm of the luminosity and its error. The asterisk in col. (1) indicates the regions that fulfil the imposed quality criterion (see § 3).

photometry error introduced by the flux calibration, since they would affect all H II regions by the same amount. Also, we did not take into account the error caused by the subtraction of the diffuse emission model (see Paper I). Since this model was smooth, it could not give raise to important relative differences for different H II regions and in any case, the subtraction error would always be much smaller than the Poissonian noise corresponding to the diffuse emission of NGC 4449.

The measured parameters are radial velocity (v_{rad}), velocity dispersion (σ), radius at a level 3 times higher than the standard deviation of the local background (R), radius corresponding to the half width at half maximum of the luminosity profile (R_F), surface brightness (SB), flux (F) and luminosity (L).

With respect to the parameters R, R_F, and L, a first error component was the standard error propagation of the image Poissonian noise (Bland, Taylor, & Atherton 1987) due to the extrapolation of the H II region luminosity profiles.

Another error source for these parameters was due to the different R, R_F, and L-values found for the H II regions located in the overlapping area of the two data cubes obtained in each emission line. In the catalog presented in

TABLE 2

H II Region Integrated Parameters for the [O III] Data

Id. (1)	v_{rad} (km s^{-1}) (2)	σ (km s^{-1}) (3)	$\epsilon(\sigma)$ (km s^{-1}) (4)	R (pc) (5)	$\epsilon(R)$ (pc) (6)	R_F (pc) (7)	$\epsilon(R_F)$ (pc) (8)	log SB (ergs s^{-1} pc^{-2}) (9)	log F (ergs s^{-1} cm^{-2}) (10)	log L (ergs s^{-1}) (11)	ϵ(log L) (ergs s^{-1}) (12)
86.....	230.0	11.4	2.3	36.2	4.5	24.4	3.3	34.3	−13.6	37.9	1.7
* 89	211.4	14.8	2.2	56.3	4.2	32.8	2.5	34.6	−13.1	38.3	0.3
*108	225.6	14.9	2.2	63.0	4.2	32.0	2.4	34.8	−12.8	38.6	0.1
*114	233.4	13.4	2.2	68.0	4.2	37.0	2.4	34.7	−12.9	38.6	0.2
*119	217.9	12.1	2.2	67.2	4.3	35.5	2.5	34.7	−12.9	38.6	0.1
128–129	223.5	24.3	2.7	50.5	4.4	37.9	3.3	34.2	−13.3	37.5	0.9
*132	225.6	13.7	2.2	84.6	4.2	39.1	2.3	35.0	−12.5	39.0	0.1
*133	207.2	15.8	2.2	74.4	4.2	35.9	2.4	35.0	−12.6	38.9	0.1
*146	215.7	21.6	2.3	94.4	5.5	65.4	4.7	34.3	−12.8	38.7	0.1
149	208.6	37.9	2.4	63.8	11.9	40.5	9.2	34.4	−13.1	38.3	0.3
151	222.9	28.1	2.3	76.8	7.9	48.3	5.9	34.4	−12.9	38.6	0.2
*153–159.....	215.3	27.4	2.2	74.3	5.2	50.0	4.1	34.3	−13.0	38.5	0.2
178–190	223.6	31.1	2.4	75.8	17.0	64.4	19.2	34.0	−13.0	38.4	0.3
191	203.8	17.8	2.6	51.5	4.7	36.4	3.9	34.2	−13.3	37.7	0.7
*203	192.3	21.7	2.3	86.1	4.5	54.2	3.0	34.4	−12.8	38.6	0.1
*208	196.8	21.9	2.3	60.5	4.2	33.3	2.4	34.6	−13.0	38.4	0.2
210	225.3	40.4	2.5	30.5	8.6	24.1	12.6	34.1	−13.8	37.7	1.2
*212	214.2	20.5	2.2	72.7	4.3	42.7	2.6	34.5	−12.9	38.5	0.2
*220	188.4	17.7	2.2	94.7	5.0	43.0	2.8	35.1	−12.3	39.2	0.0
*222	210.9	23.0	2.2	127.2	8.4	62.2	4.6	34.9	−12.2	39.3	0.1
223	194.3	29.5	2.6	37.8	28.8	27.5	20.9	34.2	−13.6	37.9	1.6
226	207.2	21.1	2.3	125.4	50.8	63.1	26.9	34.8	−12.3	39.0	0.4
*h 66	200.6	23.1	2.2	120.9	12.6	58.1	6.6	34.9	−12.2	39.3	0.1
*Nucleus.....	230.9	27.9	2.2	155.2	4.2	69.3	2.3	35.2	−11.8	39.6	0.0

Note.— Columns: (1) identification number, (2) radial velocity, (3)–(4) velocity dispersion and velocity dispersion error, (5)–(6) radius at a level 3 times higher than the standard deviation of the local background and error, (7)–(8) radius corresponding to the half width at half maximum of the luminosity profile and error, (9) logarithm of the surface brightness, (10) logarithm of the flux, (11)–(12) logarithm of the luminosity and error.

Tables 1 and 2, the values for these regions are the corresponding averages. The differences found between the two data cubes were always below 20% of the corresponding parameter. The way to consider these errors consisted of obtaining a mean value for the difference between the first and second data cube for each parameter in each spectral line, averaging the corresponding data of all the H II regions that were found in the overlapping area. Given the relatively low dispersion around these mean values, they were considered to be representative for all the H II regions in our sample, including the ones outside the overlapping area.

Since the two error sources were independent, they were quadratically added to get the final error shown in Tables 1 and 2.

Regarding the velocity dispersion, we calculated the standard error propagation due to the units conversion (from planes in the data cube to km s^{-1}) and to the correction for thermal, instrumental, and (in the case of Hα) intrinsic line broadenings.

Again, the velocity dispersion values for the nebulae in the overlapping area were slightly different for each of the two data cubes taken in each emission line. The velocity dispersion differences were always below 4.5 km s^{-1} and for the majority of the H II regions were smaller than 2 km s^{-1} (or 10% of the line width) in both emission lines. In the same way as before, an average difference value for each spectral line was adopted for all H II regions.

Another error source was caused by obtaining the velocity dispersion values from spectra extracted from the brightest part of each nebula (the one detected by FOCAS) and associating them to parameters which involve the whole nebulae (such as R or L). This method was followed in order to be reasonably sure that we were not mixing emission from adjacent nebulae in our spectra. In order to quantify this error, we extracted integrated spectra from growing concentric areas for several isolated H II regions, until the whole nebular emission had been included. The result was that for spectra extracted from areas bigger than the central 5 × 5 pixels (1.″3 × 1.″3), the velocity dispersion differences were smaller than 3 km s^{-1}. Although it is known that the H II regions kinematical parameters change considerably across its surface (Hippelein 1986; Muñoz-Tuñón 1994; Sabalisck et al. 1995), this effect is only observable in the nearest galaxies, because of the necessary spatial resolution. Since this error could only be determined for the few H II regions which were isolated enough from their neighbors, an average conservative value of 3 km s^{-1} was assumed for all the H II regions present in our sample.

The three error sources considered for the velocity dispersion are independent and so they were quadratically added in order to determine the global errors presented in Tables 1 and 2.

In this way, Tables 1 and 2 present the compiled catalog of all H II regions found in the galaxy NGC 4449 from Paper I, together with the errors determined for the corresponding parameters.

In the tables, column (1) gives the identification number, following in all cases except h61 and h66 (Hodge 1969), the catalog by Sabbandin & Bianchini (1979); column (2) lists the radial velocity. Columns (3) and (4) list the velocity dispersion (σ) and also its determined error. The velocity dispersion is the emission line(s) measured σ-value after cor-

recting for instrumental and thermal broadening. The radius at a level 3 times higher than the standard deviation of the local background and its associated error are listed in columns (5) and (6). The radius corresponding to the half width at half maximum of the luminosity profile and its error are given in columns (7) and (8). The logarithm of the surface brightness and the logarithm of the flux are given in columns (9) and (10) and the logarithm of the luminosity and its error are shown in columns (11) and (12). More details about Table 1 and Table 2 are given in Paper I.

The Hα and [O III] selected samples differ in number because many of the H II regions do not present in [O III] a detectable emission above the diffuse galactic radiation.

3. DATA ANALYSIS—THE EMPIRICAL CORRELATIONS IN NGC 4449

Once the H II regions have been cataloged and before going any further exploring the relationships between their velocity width, size, and luminosity, an analysis of the "quality" of the emission-line profiles was done. The measured velocity dispersion in a spectrum with low S/N is affected by large errors. The errors affecting our data are Poissonian (Bland et al. 1987), then the S/N is proportional to $(\mathrm{Flux})^{1/2}$, and therefore the total flux measured was taken as a S/N indicator. After a detailed visual inspection of the spectra corresponding to each region, those with an Hα flux below 1.2×10^{-13} ergs cm^{-2} s^{-1} or an [O III] flux below 7.4×10^{-14} ergs cm^{-2} s^{-1} were discarded from the set of high S/N H II regions. Also, on those nebulae showing asymmetric or split profiles, the σ-value, measured by the fitting of one single Gaussian, is clearly badly defined. Moreover, an asymmetric or a split profile may be the result of several H II regions overlapped along a line of sight. This may be a critical point in the case of galaxies, such as NGC 4449, with such a high density of nebulae. The line symmetry was calculated with MATADOR, using the procedure described by Heckman et al. (1981). This procedure can be summarized as defining a *central* wavelength for a given spectral line as the profile midpoint at 80% of intensity. From this *central* wavelength, the right and left widths at 20% and 50% of intensity are measured. Their differences constitute the profile *asymmetry* parameters which we used to define the line "quality."

The highest allowed line profile asymmetry values to include a particular region in our sample were 0.14 for the value at 20% intensity and 0.08 for that at 50% intensity. These values are necessarily arbitrary, depending also on the data quality, and come from the necessity to define a value to be used in the data analysis algorithms to quantify the goodness of a line profile. Figure 1 shows examples of discarded and accepted line profiles from the H II regions in NGC 4449.

The analysis was carried out independently for both Hα and [O III], and the resulting subsample of H II regions that fulfilled the criteria of line quality described above are indicated with an asterisk in Tables 1 and 2. Note that despite the S/N threshold and line profile quality, the remaining subsample comprises the highest surface brightness and most luminous regions of all cataloged H II regions in NGC 4449.

Figure 2 shows the size versus velocity width, both for Hα and [O III] for all cataloged regions. The two plots on the left-hand side use the radius, R, in parsecs, defined at 3 times the background standard deviation. The radius considered on the two right-hand plots, R_F, is that measured at half maximum of the luminosity profile. Full symbols correspond to the H II regions subsample, with symmetric emission lines and good S/N (marked with an asterisk in Tables 1 and 2). Triangles represent regions with a subsonic velocity dispersion. Symbols size is scaled to surface brightness (see Tables 1 and 2). Point errors have been calculated following the procedure described in § 2.

Figure 3 shows the log of the luminosity (ergs s^{-1}) versus velocity dispersion, plotted for Hα and [O III] for all cataloged regions. Symbols follow the same criterion as Figure 2. Full symbols correspond to the H II regions subsample, with symmetric emission-lines and good S/N (marked with an asterisk in Tables 1 and 2). Triangles represent regions with a subsonic velocity dispersion. Symbols size is scaled to surface brightness.

Note that regions with the "best quality profiles" (*filled points*, Figs. 2 and 3), fall on the upper part of the diagrams. They are the largest ($R \geq 50$ pc, $R_F \geq 25$ pc) and more luminous [$\log L(\mathrm{ergs\ s^{-1}}) \geq 38.5$] across the full σ range. The error in σ tends to increase as one moves toward the lower left corner of the diagrams and the errors in the ordinate (either R, R_F, or L) are also larger the smaller the radius or the smaller the luminosity of a particular H II region is. Thus, smaller and/or less luminous regions have a lower S/N and all their derived parameters are affected by larger uncertainties.

Without a doubt, the most important result that follows from the plots presented in Figures 2 and 3, is that only those regions with high surface brightness present a significant correlation among the various parameters. A similar behavior was found in the spiral galaxy NGC 4321, in which, only after restricting the sample to nebulae with the highest surface brightness, the L-σ correlation became evident (see Arsenault et al. 1990). In this respect, the discarding of sources because they may not present symmetric Gaussian profiles was found to be a second-order restriction. In our sample only one of the high surface brightness H II regions was rejected for presenting an asymmetric profile.

The range of surface brightness for the nebulae that display correlations between their integrated parameters among those already classified by having a good line profile was derived from a compromise between getting a good fit in the $\log L$-$\log \sigma$ representation and still having enough data points to define meaningful correlations. After doing so, the surface brightness (ν) threshold was set at $\log \nu_{\mathrm{H}\alpha}$ (ergs s^{-1} pc^{-2}) ≥ 35.3 and $\log \nu_{[\mathrm{O\ III}]}$ (ergs s^{-1} pc^{-2}) ≥ 34.6. This criterion was obtained in an independent way using the plots of $\log R$ and $\log R_F$ versus $\log \sigma$. The remaining H II regions from the Hα sample, that follow the correlations are: h61, SB226, h66, SB133, SB108, SB220, and the nucleus.

Then only those regions selected in [O III] that are also included in the Hα subsample were considered for the [O III] sample. The remaining regions are, SB108, h66, SB133, SB220, and the nucleus.

The resulting set of points has been fitted using a standard regression procedure, accounting for the errors in abscissas and ordinates associated to every single point. Figure 4 shows the correlations between $\log R$, $\log R_F$, and $\log L$ versus $\log \sigma$ obtained from the Hα line profiles. And Figure 5 shows the correlations obtained using the [O III] data.

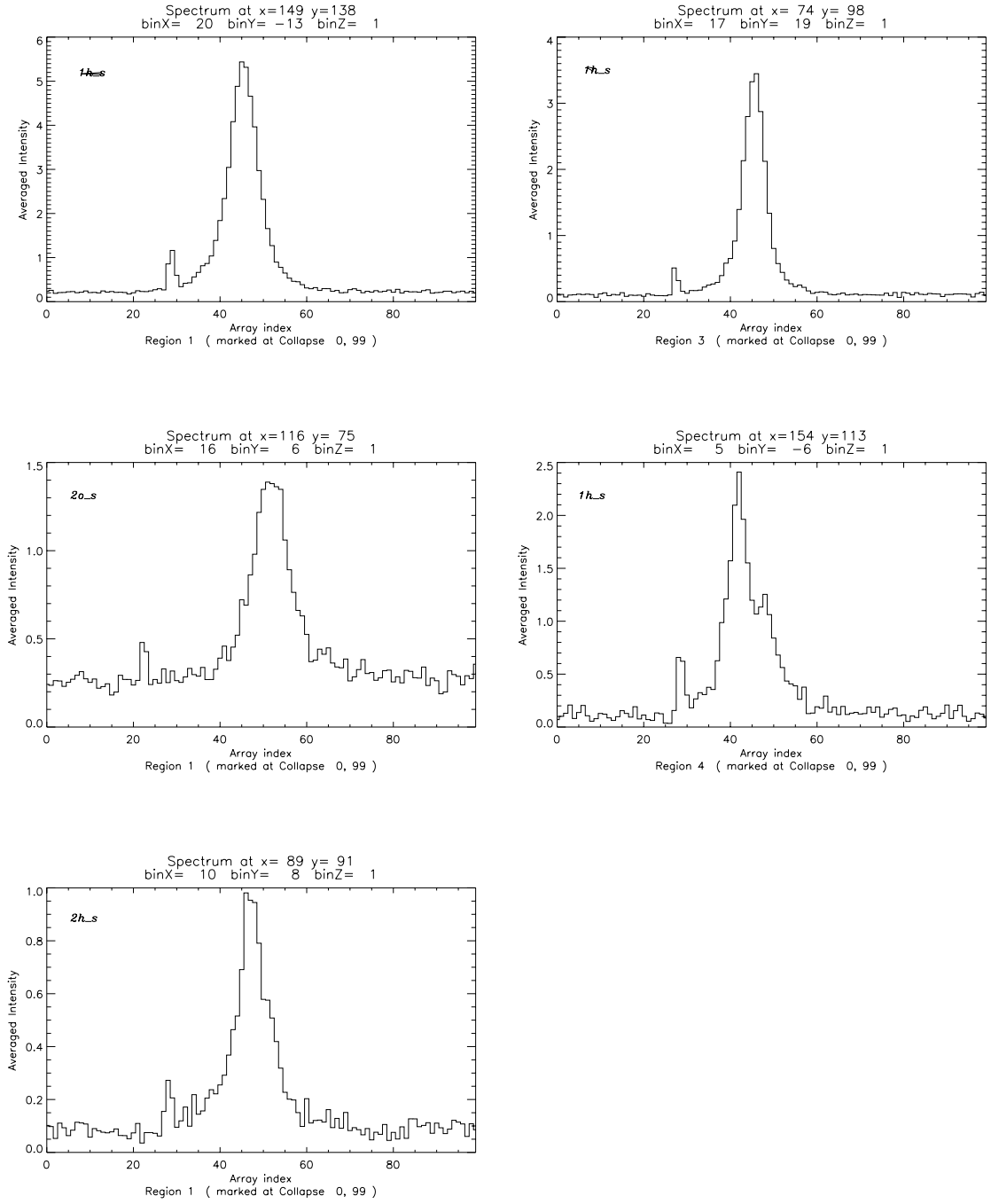

FIG. 1.—Data quality. Examples of integrated emission profiles corresponding to five cataloged regions. The first two were considered as acceptable whereas the other three were discarded for having either a poor S/N or large asymmetry coefficients. Units in abscissas are etalon planes and in the ordinates are counts in arbitrary units.

The parameters resulting from the regression, the errors and the correlation coefficients are, for Hα,

$$\log (R\ [\mathrm{pc}]) = (1.50 \pm 0.53) \log (\sigma\ [\mathrm{km\ s^{-1}}]) - (0.03 \pm 0.76),\ r = 0.866\ , \quad (1)$$

$$\log (R_F\ [\mathrm{pc}]) = (1.42 \pm 0.60) \log (\sigma\ [\mathrm{km\ s^{-1}}]) - (0.28 \pm 2.42),\ r = 0.845\ , \quad (2)$$

$$\log (L\ [\mathrm{ergs\ s^{-1}}]) = (3.75 \pm 1.17) \log (\sigma\ [\mathrm{km\ s^{-1}}]) + (34.54 \pm 1.74),\ r = 0.825\ , \quad (3)$$

and, using [O III],

$$\log (R\ [\mathrm{pc}]) = (1.30 \pm 0.27) \log (\sigma\ [\mathrm{km\ s^{-1}}]) + (0.31 \pm 0.39),\ r = 0.985\ , \quad (4)$$

$$\log (R_F\ [\mathrm{pc}]) = (1.14 \pm 0.25) \log (\sigma\ [\mathrm{km\ s^{-1}}]) + (0.19 \pm 0.35),\ r = 0.996\ , \quad (5)$$

$$\log (L\ [\mathrm{ergs\ s^{-1}}]) = (3.20 \pm 0.71) \log (\sigma\ [\mathrm{km\ s^{-1}}]) + (34.98 \pm 1.02),\ r = 0.962\ , \quad (6)$$

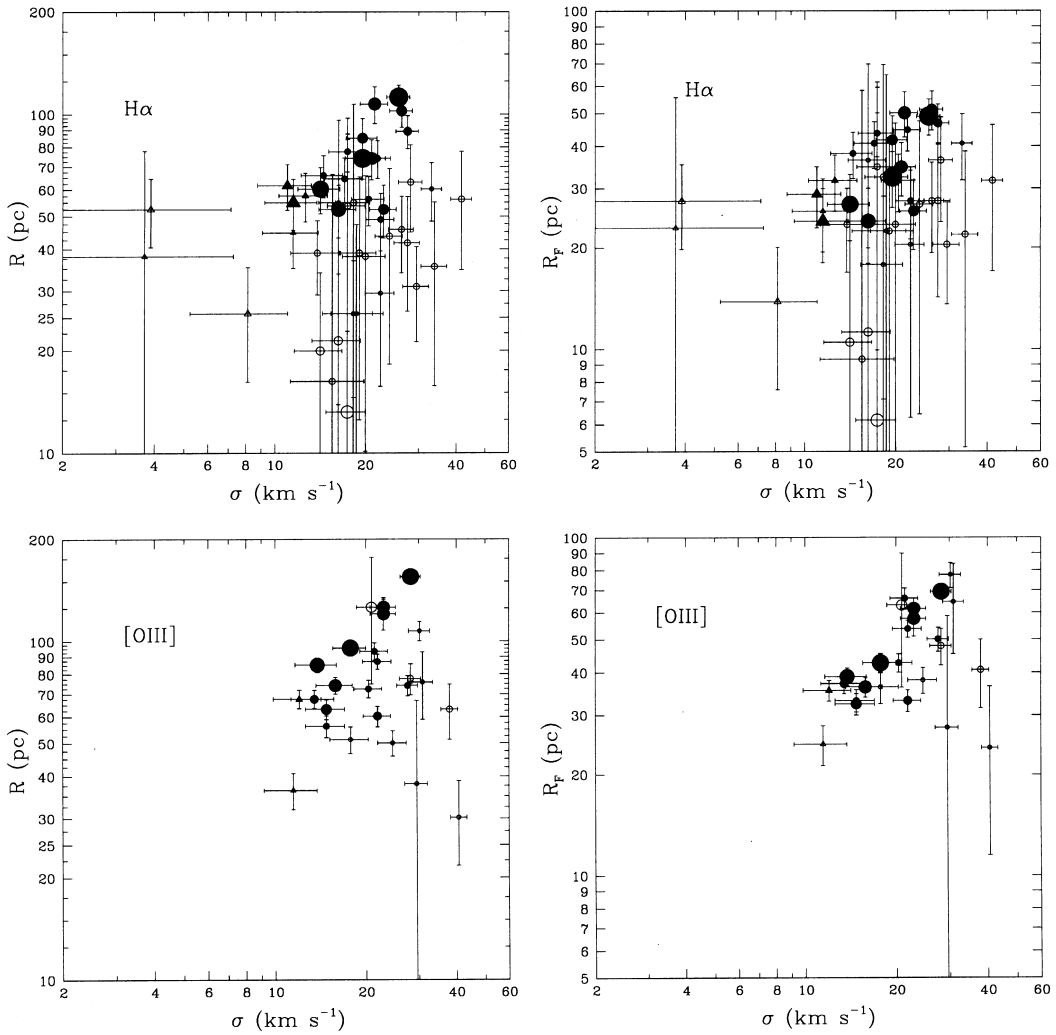

FIG. 2.—The log R vs. log σ plane. Log size (R and R_F) vs. log σ measured in Hα (*top two plots*) and [O III] (*bottom plots*) for all cataloged regions. Filled symbols correspond to regions with symmetric line profiles and good S/N. Triangles represent regions with subsonic velocity dispersion. Symbol-size scales with the measured surface brightness.

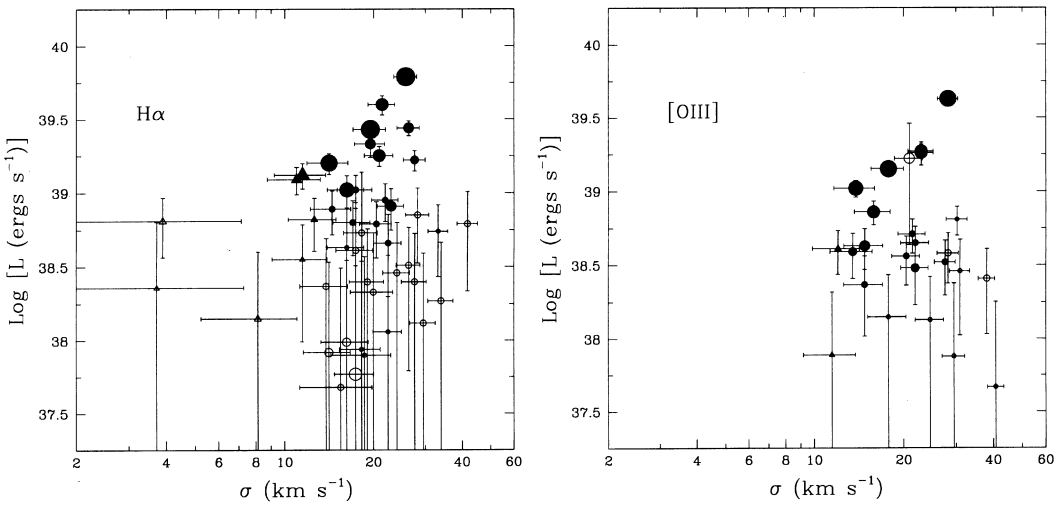

FIG. 3.—Log(L) versus log σ plane. Luminosity and σ determined from the Hα and [O III] emission lines for all cataloged regions. Filled symbols correspond to regions with good emission-line profiles, e.g., symmetric line-profiled with good S/N. Triangles represent regions with subsonic velocity dispersion. Symbol-size scales with the measured surface brightness.

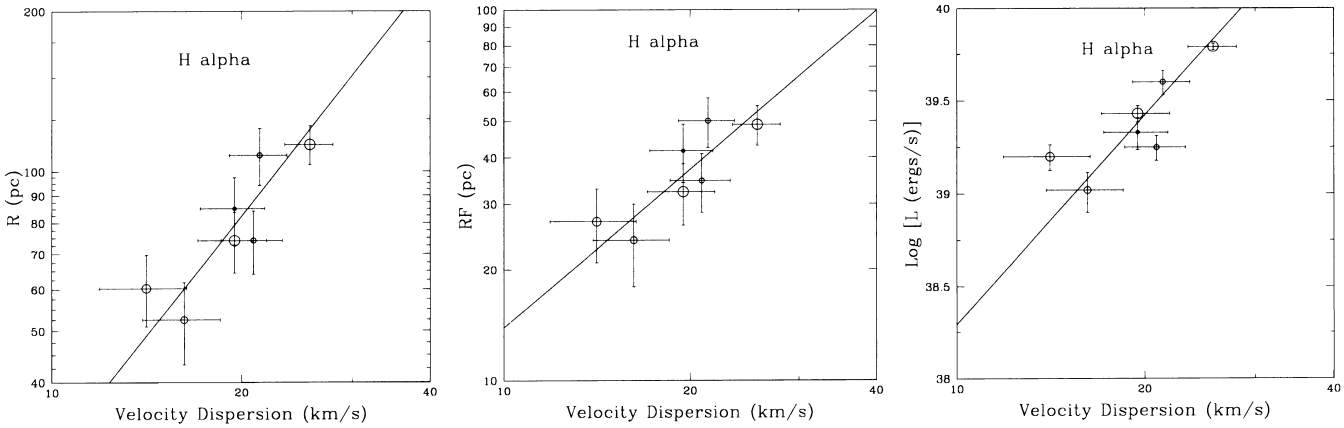

FIG. 4.—The size and luminosity vs. σ correlations in NGC 4449, from the Hα data. The correlation between log R and log σ (*left*), log R_F, and log σ (*center*) and log $L$and log σ (*right*) for the regions of highest surface brightness, with symmetric spectral profiles and good S/N, measured in Hα.

4. COMPARISON WITH OTHER STUDIES

Tables 3, 4, and 5 list a full comparison of the results obtained by different groups, including this work. In Table 3, we list the considered range of radius (parsecs), the range in σ, the resultant slope, the goodness of the correlation, and the number of objects used in each study.

Similarly Tables 4 and 5 list the considered range in luminosity, the corresponding range of σ-values, the resultant slope, the correlation coefficient, the number of considered sources, and the reference.

Given the large uncertainties associated to the different regression fits and different data sets, it can be considered that the derived correlations for the giant H II regions of NGC 4449 are in agreement with those in the literature and in particular with the gravitational models (see § 1). Some of the discrepancies can be understood for the reasons given as follows.

1. The uncertainty in the distance derived to different galaxies. This is particularly a source of error in all the studies that have considered the first ranked H II

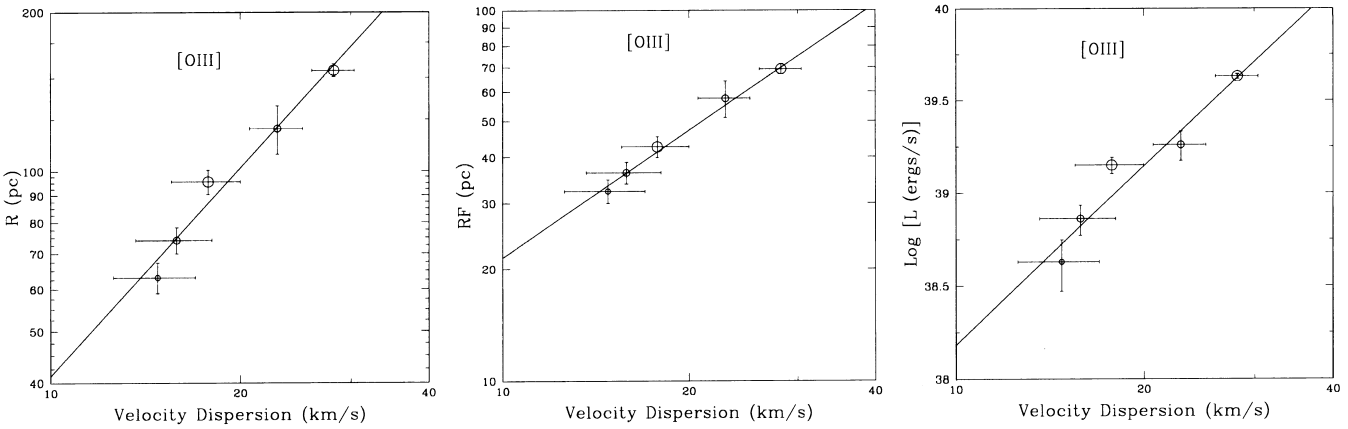

FIG. 5.—Size and luminosity vs. σ correlations in NGC 4449, from the [O III] data. The correlation between log R and log σ (*left*), log R_F and log σ (*center*) and log $L$and log σ (*right*) for the regions of highest surface brightness, with symmetric spectral profiles and good S/N, measured in [O III].

TABLE 3

SUMMARY OF RESULTS CONCERNING SIZE VERSUS σ RELATIONSHIP

Reference	Radius Range (pc)	σ Range (km s^{-1})	Equation	Corr. Coef.	No. Points
M77	27–283	9.3–23.9	$\log \langle R_c, R_h \rangle = (2.2 \pm 0.19) \log \sigma - (0.67 \pm 0.29)$	...	16
T&M81	14–165	9.3–31.0	$\log R_c = 1.84 \log \sigma - 0.47$	...	22
R.et al.86.....	33–900	9.5–29.5	$\log R_{i/v} = (1.56 \pm 0.27) \log \sigma + (0.36 \pm 0.43)$	0.65	47
M.et al.87	10–168	9.5–22.4	$\log R_c = (3.68 \pm 0.27) \log \sigma_x - (2.77 \pm 0.27)$	0.76	22
A&R88.....	24–900	9.5–29.5	$\log R_{i/v} = (1.84 \pm 0.27) \log \sigma + (0.00 \pm 0.24)$	0.68	52
This work.....	53–113	14.1–25.9	$\log R_{H\alpha} = (1.50 \pm 0.53) \log \sigma - (0.03 \pm 0.76)$	0.87	7
This work.....	24–51	14.1–25.9	$\log R_{F\ H\alpha} = (1.42 \pm 0.6) \log \sigma - (0.28 \pm 2.42)$	0.85	7
This work.....	63–155	14.9–27.9	$\log R_{[O\ III]} = (1.30 \pm 0.27) \log \sigma_{[O\ III]} + (0.31 \pm 0.39)$	0.99	5
This work.....	32–69	14.9–27.9	$\log R_{F\ [O\ III]} = (1.14 \pm 0.25) \log \sigma_{[O\ III]} + (0.19 \pm 0.35)$	0.996	5

TABLE 4

SUMMARY OF PARAMETERS CONCERNING THE LUMINOSITY VERSUS σ RELATIONSHIPS

Reference	Emission Line	σ Range (km s^{-1})	L Range (ergs s^{-1})	Corr. Coef.	No. Points
Melnick 1979	Hβ	9.3–23.9	6.0×10^{37}–8.6×10^{39}	...	16
T&M81	Hβ	9.3–31.0	3.7×10^{37}–1.6×10^{41}	...	22
R.et al.86	Hα	9.5–29.5	Not given	0.61	26
Hippelein 1986	Hα	10.3–29.8	9.1×10^{37}–3.2×10^{40}	0.66	43
M.et al.87	Hβ	9.5–22.4	3.9×10^{37}–7.1×10^{39}	0.89	22
A&R88	Hα	9.5–29.5	1.0×10^{38}–8.7×10^{40}	0.65	57
Arsenault et al. 1990	Hα	5.4–32.3	1.8×10^{37}–3.6×10^{39}	0.77	31
Rozas et al. 1998	Hα	10–80	1.0×10^{38}–2.4×10^{39}	...	140
This work	Hα	14.1–5.9	1.0×10^{39}–6.2×10^{39}	0.83	7
This work	[O III]	14.9–27.9	4.1×10^{38}–4.3×10^{39}	0.96	5

NOTE.—. M77 from Melnick 1977, T&M81 from Terlevich & Melnick 1981, R.et al.86 from Roy et al. 1986, M.et al.87 from Melnick et al. 1987, A&R88 from Arsenault & Roy 1988. T&M81 and Rozas et al. 1998 do not give error values. Radii are expressed in parsecs and velocity dispersions in km s^{-1}. Except when the opposite is indicated, σ corresponds to the Hα line width. σ_x is the average of Hα and [O III] line widths. $\langle R_c, R_h \rangle$ is the average of the core (R_c) and halo (R_h) radii as measured by Sandage & Tammann (1974). $R_{i/v}$ corresponds to works where some nebular sizes are isophotal while others were visually determined.

regions in different galaxies. Note that Roy et al. (1986) obtained largely different correlation slopes, both for the size versus σ and for the L versus σ correlations, if they considered the distance to their 26 objects to be those found by Richter & Hutchmeier (1984), i.e., $\log R = (1.56 \pm 0.27) \log \sigma - (0.36 \pm 0.43)$ and $\log L = (3.15 \pm 0.83) \log \sigma + (35.37 \pm 1.29)$, or the ones given by Bottinelli et al. (1984) which led to $\log R = (0.68 \pm 0.28) \log \sigma + (1.23 \pm 0.43)$ and $\log L = (0.87 \pm 0.99) \log \sigma + (37.86 \pm 1.52)$.

2. The regression algorithms used are not the same in all studies. In some cases (as in Melnick 1977, Roy et al. 1986, and Arsenault et al. 1990) the errors in the radii and luminosity of the sources are not considered. While in the present study, the same as Hippelein (1986) and Melnick et al. (1987) the errors in all the physical variables involved are taken into consideration. Large differences result from accounting or not of the abscissas and/or ordinates errors. Melnick et al. for example found that $\log R = (3.68 \pm 0.27) \log \sigma - (2.77 \pm 0.27)$ and $\log L = (4.92 \pm 0.30) \log \sigma + (33.24 \pm 0.31)$ from a regression that takes the x and y errors into consideration, and $\log R = (2.64 \pm 0.51) \log \sigma - (1.42 \pm 0.61)$ and $\log L = (4.17 \pm 0.47) \log \sigma + (34.12 \pm 0.56)$ when they are not.

3. The different definitions of size. The different definitions of H II region size adopted by the various groups are not directly comparable. This, given the small range of log R covered by the observations, has a significant impact on the derived correlations. Clearly, visual estimates of the size are less reliable than the isophotal-derived dimensions. A clear example of this can be found when comparing the results of Roy et al. (1986) who found $\log R = (1.56 \pm 0.27) \log \sigma + (0.36 \pm 0.43)$ and those of Melnick et al. (1987) who found $\log R = (2.64 \pm 0.51) \log \sigma - (1.42 \pm 0.61)$, even when the latter used a regression algorithm similar to Roy et al. (1986).The sizes determined by Melnick et al. (1987) seem to grow faster than the isophotal ones determined by Roy et al. (1986). The slopes derived in our study seem to be closer to those derived from an isophotal determination of the radius.

4. The different adopted values of σ. Hippelein (1986) uses in one case $\sigma_{\rm O\,III}$, that systematically differs by 2 km s^{-1} from his $\sigma_{\rm H\alpha}$-values. The use of a different σ, including the average value [0.5 ($\sigma_{\rm O\,III} + \sigma_{\rm H\alpha}$) or σ_x], leads also to significant differences in the slope of the correlation.

TABLE 5

SUMMARY OF RELATIONSHIPS FOUND BETWEEN LUMINOSITY AND σ[a]

Reference	Equation
Melnick 1979	$\log L(\mathrm{H}\beta) = (4.2 \pm 1.2) \log \sigma + (33.5 \pm 1.6)$
T&M81	$\log L(\mathrm{H}\beta) = 4.0 \log \sigma + 34.0$
R.et al.86	$\log L(\mathrm{H}\alpha) = (3.2 \pm 0.8) \log \sigma + (35.4 \pm 1.3)$
Hippelein 1986	$\log L(\mathrm{H}\alpha) = (6.6 \pm 0.4) \log \sigma + (31.1 \pm 0.3)$
Hippelein 1986	$\log L(\mathrm{H}\alpha) = (5.9 \pm 0.3) \log \sigma_{\rm [O\,III]} + (32.3 \pm 0.3)$
M.et al.87	$\log L(\mathrm{H}\beta) = (4.9 \pm 0.3) \log \sigma_x + (33.2 \pm 0.3)$
A&R88	$\log L(\mathrm{H}\alpha) = (3.9 \pm 0.6) \log \sigma + (34.6 \pm 0.6)$
Arsenault et al 1990	$\log L(\mathrm{H}\alpha) = (2.6 \pm 0.5) \log \sigma + (35.5 \pm 0.9)$
Rozas et al. 1998	$\log L(\mathrm{H}\alpha) = 2.6 \log \sigma + 36.2$
This work	$\log L(\mathrm{H}\alpha) = (3.8 \pm 1.2) \log \sigma + (34.5 \pm 1.7)$
This work	$\log L([\mathrm{O\,III}]) = (3.2 \pm 0.7) \log \sigma_{\rm [O\,III]} + (35.0 \pm 1.0)$

[a] Luminosities are expressed in ergs s^{-1}. Other symbols and units are the same as in Table 3.

5. The number of considered H II regions in the sample is also an important parameter. A small set of objects with a considerable dispersion in the $\log R$ versus $\log \sigma$, and the $\log L$ versus $\log \sigma$ planes, makes the correlations extremely sensitive to the accurate determination of the parameters of each of the objects.

6. The distance effect can also cause confusion between truly single and clustered H II regions, causing large variations in the slope of the correlations.

All of the above are important issues that may cause important differences in the determination of the correlations, and thus, despite the differences obtained between the correlations for the giant H II regions of NGC 4449 and those in the literature, one can regard the results as compatible. Note however, that our study has reduced the scatter in the data points, largely due to a homogeneous set of giant H II regions, all located at the same distance. We have also shown that the empirical correlations for the giant H II regions of NGC 4449 only become apparent once the sample is restricted to giant H II regions with a high surface brightness. This has also been the case in other studies, but it may have passed unnoticed, particularly in those studies concerned with first ranked H II regions in different galaxies.

5. SUMMARY AND FINAL REMARKS

From our two dimensional spectroscopic data of the giant irregular galaxy NGC 4449, obtained at the 4.2 m WHT at La Palma Observatory, we have cataloged 44 giant H II regions from their Hα emission lines and 24 from their [O III] counterparts. The main difference in number arises from the fact that many of the H II regions do not present in [O III] a detectable emission above the diffuse radiation from the galaxy. For all the detected regions we have obtained their diameter, luminosity, and surface brightness, as well as their radial velocity and velocity dispersion.

Clearly the most difficult issue is to achieve a precise determination of the parameters under consideration, namely, size, luminosity, and velocity dispersion. A very rigorous, and certainly time-consuming, procedure such as the one we have followed in Paper I, is absolutely necessary. Less accurate methods, both at the telescope and in the data analysis, may easily become limited in their scope and certainly may lead to doubtful results.

The statistical analysis of the giant H II regions in our sample has shown that the correlation between size and σ and luminosity and σ only become apparent for nebulae with a high surface brightness that also show single Gaussian supersonic emission lines. The need of a high surface brightness sample is an effect hardly noticed in previous studies owing to their bias toward first ranked giant H II regions in star-forming galaxies. Note also that the possible asymmetries of the emission lines is another effect not considered in this respect in the literature. The parameters derived for the correlations between size and σ and luminosity and σ are not in disagreement with the values derived by other groups, particularly if one considers the errors in the determination of all physical variables and the scatter around the regression curves. In this respect, the homogeneity of our sample, which considers only nebulae at identical distances, and the reliable methods used to determine all physical variables, have led to a restricted scatter of points around the regression curves.

Our results (Tables 3–5) also show that the regression curves, within the errors, are consistent with all former works supporting virialized systems as the ultimate origin of the supersonic motions. This holds despite the fact that only a small number of H II regions, among all those cataloged in NGC 4449, define the log-log relationships between their structural and intrinsic parameters. We have noticed that all of these regions surpass a surface brightness threshold, and thus the existence of the correlations may also involve the age, evolution, disruption, and expansion of the considered nebulae. The fact that the most luminous regions are the ones that best follow the defined relationships points also to a physical mechanism which should involve the whole mass of the cloud. This, together with the exponents found, favor the virial as the physical scenario behind them.

With regards to which of the two correlations is more reliable, one can think of a variety of arguments in favor of each of the structural parameters (size and luminosity). In the case of R, major improvements have led to a more reliable determination. This parameter was initially determined from visual estimates. More recently, accurate measurements of the supersonic velocity dispersion in nearby giant H II regions, has led to the determination of the extent of the regions producing supersonic single Gaussian lines. The size of such region, defined by Muñoz-Tuñón (1994) as the "kinematic core" of the giant H II regions, is perhaps the most accurate determination of such parameter. However, it implies a precise method of sampling spatially the emission lines, and thus it is only useful in nearby fully resolved systems. In the case of NGC 4449 the size of the regions was determined also in an accurate manner. Special attention was paid to decontaminate from the background diffuse emission that engulfs the galaxy. Also most care was taken to detect the possible overlap of several H II regions. The extra parameter "line-quality" here considered assures not only that misleading σ-values are not used, but also helps to discard regions which could possibly overlap along the line of sight. These in some cases may be spatially sufficiently close as to not allowing to discriminate them in the image. It is obvious that we are always limited by the spatial and spectral resolution achieved, but the method we have employed is the best possible to decontaminate from all these spurious effects.

Thus, regarding sizes, we conclude that our results for the giant H II regions of NGC 4449 hold for both R and R_F. The similarity of the results implies that any of them (R or R_F) could be used in future work.

Regarding the luminosity of the targets, we have found that the more luminous a region is, the better it fits the correlation. Note, however, that the more luminous regions may be affected by the structure of the host galaxy and the distribution of the ISM. Indeed, larger and brighter H II regions may rapidly evolve into density-bounded nebulae. In such cases, the number of detected recombinations would not balance all photons emitted by the exciting stars and thus the true luminosity will be ill determined.

On the other hand, an ionization-bounded H II region may simply reflect the fact that not all massive stars have formed. In this case, although σ may be already fully established, as in the cometary stirring model (Tenorio-Tagle et al. 1993), and well determined by accurate observations of

single Gaussian lines, the size and luminosity of the region would be underestimated.

This study was partly financed by the Spanish DGES (grant PB97-0158) and the CONACYT (México) project 28501E. The WHT and JKT are operated on the island of La Palma by the ING at the Observatorio del Roque de los Muchachos of the IAC. C. M. T. acknowledges the hospitality of the INAOE where this work was completed.

REFERENCES

Aaronson, M., & Mould, J. 1983, ApJ, 265, 1
Arsenault, R., & Roy, J. R. 1988, A&A, 201, 199
Arsenault, R., Roy, J. R., & Boulesteix, J. 1990, A&A, 234, 23
Bland, J., Taylor, K., & Atherton, P. D. 1987, MNRAS, 228, 595
Bottinelli, L., Gougenheim, L., Paturel, G., & de Vaucouleurs, G. 1984, A&AS, 56, 381
Chu, Y. H., & Kennicutt, R. C. 1994, ApJ, 425, 720
Dyson, J. E. 1979, A&A, 73, 132
Fuentes-Masip, O. 1997, Ph.D. thesis, Univ. La Laguna
Fuentes-Masip, O., Castañeda, H. O., & Muñoz-Tuñón, C. 2000, AJ, 119, 2166 (Paper I)
Gallagher, J. S., & Hunter, D. A. 1983, ApJ, 274, 141
Gavryusev, V., & Muñoz-Tuñón, C. 1996, in ASP Conf. Ser. 101, Astronomical Data Analysis Software and Systems V (San Francisco: ASP), 76
Gum, C. S., & de Vaucouleurs, G. 1953, Observatory, 73, 152
Hartmann, L. W., Geller, M. J., & Huchra, J. P. 1986, AJ, 92, 1278
Heckman, T. M., Miley, G. K., van Breugel, W. J. M., & Butcher, H. R. 1981, ApJ, 247, 403
Hippelein, H. H. 1986, A&A, 160, 374
Hodge, P. W. 1969, ApJS, 18, 73
———. 1976, ApJ, 205, 728
———. 1983, AJ, 88, 1323
Kennicutt, R. C. 1979, ApJ, 228, 394
———. 1984, ApJ, 287, 116
———. 1988, ApJ, 334, 144
Malumuth, E. M., Williams, T. B., & Schommer, R. A. 1986, AJ, 91, 1295
Melnick, J. 1977, ApJ, 213, 15
———. 1979, ApJ, 228, 112
Melnick, J., Moles, M., Terlevich, R., & García-Pelayo, J. M. 1987, MNRAS, 226, 849
Melnick, J., Tenorio-Tagle, G., & Terlevich, R. 1999, MNRAS, 302, 677
Melnick, J., Terlevich, R., & Moles, M. 1988, MNRAS, 235, 297
Muñoz-Tuñón, C. 1994, in Violent Star Formation: From 30 Doradus to QSOs, ed. G. Tenorio-Tagle (Cambridge: Cambridge Univ. Press), 25
Muñoz-Tuñón, C., Gavryusev, V., & Castañeda, H. O. 1995, AJ, 110, 1630
Muñoz-Tuñón, C., Tenorio-Tagle, G., Castañeda H. O., & Terlevich, R. 1996, AJ, 112, 1636
Richter, O. G., & Hutchmeier, W. K. 1984, A&A, 132, 253
Roy, J. R., Arsenault, R., & Joncas, G. 1986, ApJ, 300, 624
Rozas, M., Sabalisck, N., Beckman, J. E., & Knapen, J. H. 1998, A&A, 338, 15
Sabalisck, N. S. P., Tenorio-Tagle, G., Castañeda, H. O., & Muñoz-Tuñón, C. 1995, ApJ, 444, 200
Sabbandin, F., & Bianchini, A. 1979, PASP, 91, 280
Sandage, A., & Tammann, G. A. 1974, ApJ, 190, 525
———. 1975, ApJ, 196, 313
Sérsic, J. L. 1960, Z. Astrophys., 50, 168
Smith, M. G., & Weedman, D. W. 1970, ApJ, 161, 33
Tenorio-Tagle, G., Muñoz-Tuñón, C., & Cid-Fernandes, R. 1996, ApJ, 456, 264
Tenorio-Tagle, G., Muñoz-Tuñón, C., & Cox, D. P. 1993, ApJ, 418, 767
Terlevich, R., & Melnick, J. 1981, MNRAS, 195, 839